

Vibrational Modes in Strongly Deformed Nuclei

Y. Tsunoda,^{1,2,*} T. Otsuka,^{3,4,5,6,†} N. Shimizu,² T. Duguet,⁷ Y. Utsuno,⁸ and T. Abe⁹

¹Center for Nuclear Study, The University of Tokyo, 7-3-1 Hongo, Bunkyo, Tokyo 113-0033, Japan

²Center for Computational Sciences, University of Tsukuba, 1-1-1 Tennodai, Tsukuba, Ibaraki, 305-8577, Japan

³Department of Physics, The University of Tokyo, 7-3-1 Hongo, Bunkyo, Tokyo 113-0033, Japan

⁴RIKEN Nishina Center, 2-1 Hirosawa, Wako, Saitama 351-0198, Japan

⁵Grand Accélérateur National d'Ions Lourds, CEA/DRF-CNRS/IN2P3, Bvd Henri Becquerel, F-14076 Caen, France

⁶Institut für Kernphysik, Technische Universität Darmstadt, D-64289 Darmstadt, Germany

⁷IRFU, CEA, Université Paris-Saclay, 91191, Gif-sur-Yvette, France

⁸Advanced Science Research Center, Japan Atomic Energy Agency, Tokai, Ibaraki 319-1195, Japan

⁹Quantum Computing Center, Keio University, 3-14-1 Hiyoshi, Kohoku-ku, Yokohama, Kanagawa 223-8522, Japan

(Dated: July 29, 2025)

Low-energy vibrational excitations associated with the fluctuation of quadrupole deformed shapes are discussed within the frame of state-of-the-art Configuration Interaction calculations, actually performed via the Quasi-particle Vacua Shell Model version of the Monte Carlo Shell Model. Recently, low-lying γ bands in heavy strongly deformed nuclei were shown to be rotational $K^P = 2^+$ excitations of triaxially deformed states (see T. Otsuka *et al.*, Eur. Phys. J. A 61, 126 (2025)) rather than vibrational excitations as traditionally interpreted. In this context, it is important to identify possible low-lying vibrational excitations and to characterize the excitation energy at which they emerge. Focusing on two typical examples, ¹⁶⁶Er and ¹⁶²Dy, vibrational states are indeed identified above the γ band using an extended version of the so-called T-plot. The phenomenon of shape coexistence is also shown to produce low-lying states below such vibrational band heads. These results suggest novel and rich structures in heavy deformed nuclei. While experimental counterparts are seen for some of such states, others are predictions opening doors to future dedicated experiments.

Low-energy rotational excitations emerge in nuclei characterized by strongly deformed ellipsoidal shapes, as pointed out early on by Rainwater [1], as well as by Bohr and Mottelson [2–4]. Properties associated with strong deformation were discussed in many works afterwards as described in textbooks, e.g. see Refs. [5–11]. Complementarily, low-energy vibrational excitations arise in various situations, including in nuclei characterized by deformed ellipsoidal shapes. Well-known examples are β - and γ -vibrations [3, 5]. There have been many extensive studies of vibrational modes, as also documented in the textbooks mentioned above.

Recently, a systematic investigation of strongly deformed quadrupole shapes and associated rotational excitations was performed in heavy ($A = Z + N > 140$) nuclei with even neutron (N) and proton (Z) numbers [12, 13]. This was achieved using state-of-the-art ultra-large-scale Configuration Interaction (CI) calculations performed within the frame of the Quasi-particle Vacua Shell Model (QVSM) [14] version of the Monte Carlo Shell Model (MCSM) [15, 16]. In such a study, the band head of so-called γ bands, which is traditionally interpreted as γ vibration, has been convincingly shown to rather be the $K^P = 2^+$ rotational excitation of a triaxially deformed ground state. This change of perspective poses the question, addressed in the present Letter, of the emergence of low-lying vibrational excitations in such heavy strongly deformed nuclei. To do so, the MCSM calculation is extended with additional MCSM basis vectors compared to earlier studies focusing on rotational states, with

the goal to target vibrational states of quadrupole character at excitation energies below ~ 3 MeV. The goal is to uncover novel features exhibited by vibrational excitations [5–11, 17] and shape-coexistence phenomena [18–21]. To do so, ¹⁶⁶Er and ¹⁶²Dy are presently used as typical illustrative examples.

The MCSM [15, 16] solves the many-body Schrödinger equation within a designated many-body Hilbert space built on top of a frozen core based on a valence single-particle space in which a given number of valence nucleons interact via an effective two-nucleon (2N) interaction. The valence proton (neutron) space used in the present calculation collects single-particle states belonging to the *sdg(pfh)* harmonic-oscillator (HO) shell plus the lower half of the next shell, i.e. it is made of the one-and-half HO shell on top of a ¹¹⁰Zr inert core. The dimension of the many-body Hilbert space is about 10^{33} , which is formidably larger than the current limit ($\sim 10^{11}$) of the conventional CI codes. The proton-proton and neutron-neutron channels of the 2N interaction are taken from Ref. [22] and completed by the V_{MU} interaction [23] for matrix elements not covered by this recipe. The V_{MU} interaction, also used for the proton-neutron channel (including a slight modification), was determined as a simple modeling [23] for systematic studies of Zr, Sn, Nd, Sm and Hg isotopes [13, 24–29]. The QVSM [14] version of the MCSM [15, 16] utilizes the Bogoliubov basis vectors so that pairing correlations can be incorporated within individual basis vectors, as this is a serious problem for heavy nuclei with Slater determinants as in the usual MCSM.

For a given (J, M) value, where J (M) denotes the total angular momentum (its z -component), the k -th eigenstate reads in the QVSM as

$$|\Psi_k\rangle \equiv \sum_{iK} f_{iK}^{(k)} |\phi_{iK}\rangle, \quad (1)$$

with $f_{iK}^{(k)}$ the amplitudes of the mixing and

$$|\phi_{iK}\rangle \equiv \mathcal{P}_{MK}^J |\phi^{(i)}\rangle, \quad (2)$$

the i -th MCSM basis vector. The latter is obtained by projecting the triaxially deformed number-projected Bogoliubov state $|\phi^{(i)}\rangle$ onto good J, M (parity projection is also included, but not explicitly shown for brevity) via the symmetry projection operator \mathcal{P}_{MK}^J . The integer K runs from $-J$ to J and thus corresponds to independent basis vectors for a given set of J and M values.

Although the geometrical meaning of K quantum number may be lost in general MCSM calculations via the mixing of the K values, the meaning can be restored [12] also in the present study: For strongly quadrupole deformed cases, each basis vector can be mapped on to the intrinsic state with an ellipsoidal shape, and its z axis, i.e., the longest ellipsoidal axis, can be aligned to a common direction among the basis vectors, without changing MCSM results. The K quantum number defined with this common axis exhibits a physical meaning like the simple geometrical one, and has been shown to be practically conserved in low-lying strongly deformed states with triaxiality [12]. This feature is confirmed to similarly remain in vibrational states to be discussed, and such K quantum numbers are indicated.

Figure 1 displays for ^{166}Er experimental [30] and calculated excitation energies of low-lying positive-parity states with angular momenta $J = 0, 2, 3, 4$ [57]. Selected $B(E2)$ reduced transition probabilities among some of these states are also shown. Levels below ~ 1 MeV were discussed in [12] along with the experimental 4^+ state at excitation energy $E_x = 2.028$ MeV and the calculated $J^P = K^P = 4^+$ state.

Some of these low-lying states were analyzed in the past from the viewpoint of possible triaxial shapes or so-called γ -instability, see Refs. [31–43], as well as to search for double γ -phonon ($\gamma\gamma$) $K^P = 4^+$ and $K^P = 0^+$ states in [44–46]. On the other hand, no triaxiality was suggested for strongly-deformed heavy nuclei in, for instance, Refs. [5, 47, 48]. A key point of Ref. [12] was to demonstrate that the band head of the $K^P = 2^+$ γ band relates to the rotation of a triaxial state contrary to the traditional interpretation at play. Above 1 MeV, one observes three bands that are the focus of the present work. To analyze their nature, the characteristics of a given state $|\Psi_k\rangle$ is studied below based on an extension of the so-called T-plots.

As the states $|\phi_{iK}\rangle$ are non-orthogonal among themselves, their linear combinations are taken to be orthonormal, by diagonalizing the norm matrix, resulting in the states $|\tilde{\phi}_{iK}\rangle$ comprising linear combinations of $|\phi_{iK'}\rangle$ with

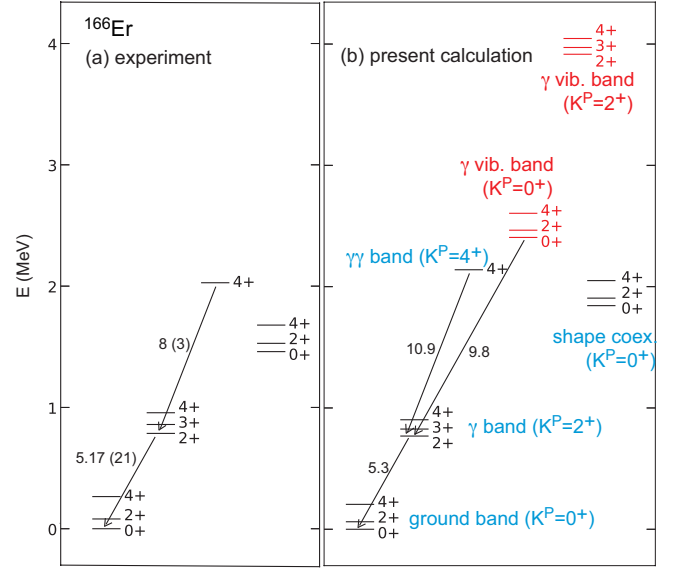


FIG. 1. Experimental [30] (a) and present theoretical (b) energy levels in ^{166}Er . Bands built on a vibrational excitation (see text) are shown in red. Many experimental levels above ~ 2 MeV are not shown whereas some theoretical levels are also omitted because of their weaker relevance. Selected $B(E2)$ values are shown in W.u.

$i' = 1, 2, \dots$ and $K' = -J, \dots, J$. We further introduce K -integrated states out of them

$$|\tilde{\phi}_i^{(k)}\rangle = \frac{1}{\mathcal{N}_i^{(k)}} \sum_K \tilde{f}_{iK}^{(k)} |\tilde{\phi}_{iK}\rangle, \quad (3)$$

where $\mathcal{N}_i^{(k)}$ is a normalization constant, and $\tilde{f}_{iK}^{(k)}$ denotes the amplitude thus determined. While this is a general expression, K is not evenly distributed but is rather concentrated in strongly deformed nuclei. These states form

$$|\Psi_k\rangle = \sum_i \mathcal{N}_i^{(k)} |\tilde{\phi}_i^{(k)}\rangle. \quad (4)$$

Given a physical state $|\Psi_k\rangle$, the T-plot displays at the value of the deformation parameters β_2 and γ of each basis vector $|\phi^{(i)}\rangle$ a circle whose area expresses the K -summed probability $|\mathcal{N}_i^{(k)}|^2 = \sum_K |\tilde{f}_{iK}^{(k)}|^2$ [58]. The T-plot was originally introduced for non-orthogonal basis vectors [49, 50], but is presently made with the orthonormality [52], in order to incorporate finer details of wave functions.

In the present work, the “Phase-specified T-plot (PT-plot)” is introduced to further incorporate information about the phase of amplitudes, $\mathcal{N}_i^{(k)}$. As the phase of the product $\tilde{f}_{iK}^{(k)} |\tilde{\phi}_{iK}\rangle$ in eq. (3) is fixed for a given eigenstate $|\Psi_k\rangle$, we extract the information provided by the pattern of this phase over various basis vectors, $|\tilde{\phi}_i^{(k)}\rangle$. To do so, a reference state $|\Psi_{k=R}\rangle$ is introduced. Then, the overlap $\langle \tilde{\phi}_i^{(R)} | \tilde{\phi}_i^{(k)} \rangle$ is calculated. This overlap characterizes the relation between the i -th basis vectors of the two eigenstates, and appears to be dominantly real, positive or negative,

in many cases of present interest as explained later. Otherwise, they are complex numbers in general. The color which the circles are filled with in the PT-plot specifies the sign of such dominating real part of the amplitude. The color is then red (yellow) for positive (negative) amplitudes. It becomes closer to white in case the situation differs.

Figure 2(a) displays the particle-number-projected Hartree-Fock-Bogoliubov (PNP-HFB) potential energy surface (PES) against β_2 and γ . Other panels show PT-plots limited to the rectangular area [59] shown in panel (a) for eight selected eigenstates analyzed against appropriate reference states.

By construction, all circles in panel (b) are red given that the 0_1^+ ground state is analyzed taking itself as the reference state $|\Psi_R\rangle$. As visible from Fig. 2(c), the PT-plot of the 0_3^+ state displays a rather similar distribution of circles aligned perpendicularly to the $\gamma = 0^\circ$ axis. However, the sign of the amplitudes changes in a characteristic way for that excited 0^+ state.

To better understand such a feature, Figs. 3 (b) and (c) depict the amplitudes of the basis vectors for both states per γ bin of 1° . The linear combination of vectors belonging to a given bin and displaying positive (negative) amplitudes are gathered together. Normalizing the corresponding vector, a positive (negative) overall amplitude is extracted and plotted as a red (yellow) histogram in Fig. 3. While only positive amplitudes arise for the 0_1^+ state in panel (b), panel (c) dedicated to the 0_3^+ state shows that each bin contains positive and negative histograms. However, red histograms strongly dominate the left-hand side (i.e. small γ values) of the distribution whereas yellow ones dominate its right-hand side.

The profile of the collective amplitudes of the 0_1^+ and 0_3^+ states as a function of γ recalls the behavior of the wave function of the first and second eigenstates of a particle in a harmonic oscillator potential schematically displayed in Fig. 3(a). While the ground state is a gaussian wave packet sitting in the center of the harmonic well, the first excited state is a one-node vibration with a change of sign at the center of the well [60]. The comparison of panels (b) and (c) with panel (a) suggests that the 0_3^+ state is itself a vibration on top of the 0_1^+ ground state, the deformation parameter γ playing the role of the coordinate of the potential. The amplitude is indeed peaked in the bin $\gamma = 8-9^\circ$ in panel (b), whereas it is quite small in the same bin in panel (c) and displays a convincing oscillation around it. It happens that vibrational excitations with seemingly similar nodal structure can appear using, e.g., the Bohr Hamiltonian with triaxiality [10, 53, 54], particularly if the potential can be approximated by a harmonic oscillator potential or a resembling one [55].

One may wonder why the γ vibration displays a 0^+ band head, rather than a 2^+ band head *à la* A. Bohr. The present γ vibrational state belongs to a set of triaxial states differing by the K quantum number. The energy splitting associated

with this K quantum number explains [12] why the $K^P = 0^+$ band is robustly lower than the $K^P = 2^+$ band for a given γ vibrational mode from a triaxial ground state.

The PT-plot of the 0_2^+ state with $E_x \sim 2$ MeV in Fig. 2(d) suggests that it is more deformed than the $0_{1,3}^+$ states and a good candidate for a shape-coexistence mechanism with respect to β_2 [18–21] with near-prolate deformation ($\gamma \sim 2^\circ$).

The PT-plot of the 2_1^+ state in panel (f) is very similar to that of the 0_1^+ state in panel (b). This relates to the fact that this state is the 2^+ excitation belonging to the ground-state rotational band.

The white circles in panel (g) indicate that the 2_1^+ state should not be used as a reference state to describe the 2_2^+ state. Indeed, the latter is the lowest $K^P = 2^+$ rotational excitation of the triaxial ground state as discussed in Ref. [12]. It is thus more appropriate to analyze that state against itself as shown in panel (h). With this at hand, panel (i) shows that, just like the 0_3^+ state is the $K^P = 0^+$ γ vibration on top of the 0_1^+ state, the 2_5^+ state is the $K^P = 2^+$ γ vibration on top of the 0_1^+ state. The 4_4^+ state displays a PT-plot similar to panel (h) with a small overall shift towards stronger triaxiality, being consistent with its $J^P = K^P = 4^+$ character [12].

Thus, real amplitudes rather distinctly emerge as a signature of vibrational excitations, while amplitudes can be complex numbers in other cases.

Remarkably, no vibrational states in the β_2 direction has been found for ^{166}Er in the excitation-energy range under scrutiny.

The 0_3^+ state, the γ -vibrational band head, decays to the 2_2^+ state with relatively large $B(E2) = 9.8$ W.u. in the present calculation. This is compatible with calculated $B(E2; 4_{\gamma\gamma}^+ \rightarrow 2_2^+) = 10.9$ W.u. This 4^+ state is labeled as “ $\gamma\gamma$ band ($K^P=4^+$)” in Fig. 1 (b), and depicts a PT-plot in panel (e) similar to panel (h), being consistent with this labeling. The decay of the 0_3^+ state with a relatively large $B(E2)$ value would be interpreted, in a traditional picture, as the decay of a double- γ -phonon state of $K^P = 0^+$ [44, 45].

Moving now to ^{162}Dy , Fig. 4 depicts experimental and calculated energies of low-lying positive-parity states with angular momenta $J = 0, 2, 3, 4$, along with selected $B(E2)$ values. Similarly to ^{166}Er , Fig. 5 displays the PNP-HFB PES and the PT-plots for a selected set of states.

Figure 5(c) depicts the PT-plot of the 0_2^+ state composed of red and yellow symbols. This is nothing but a vibrational excitation in the β_2 direction. Figure 3 (d), (e) clarifies it with an analysis similar to Fig. 3 (b), (c), the coordinate being β_2 instead of γ . Again, the 0_1^+ ground state and the 0_2^+ excited state conform well to the expected picture of a harmonic oscillator, the latter behaving as a low-lying β -vibrational excitation on top of the former [61]. This is made possible by the wider bottom of the PES in the β_2 direction for ^{162}Dy than for ^{166}Er . It is of interest to see

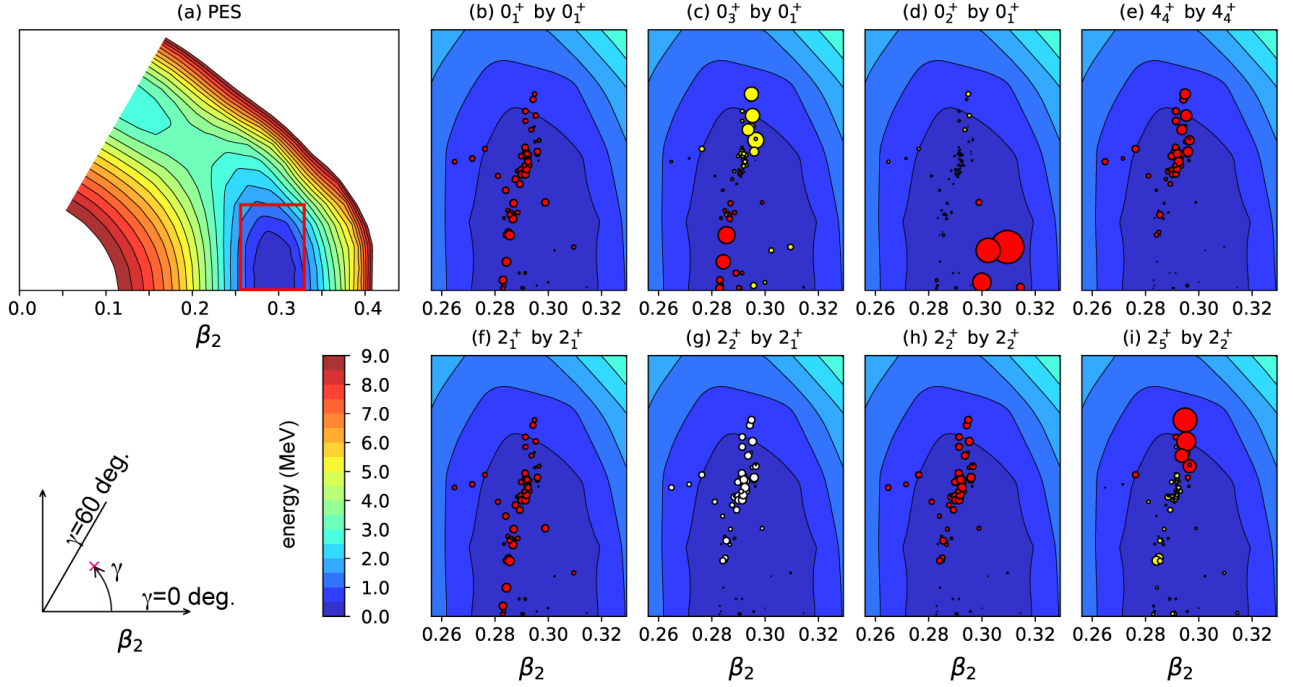


FIG. 2. Particle number projected potential energy surface (a) and phase-specified T-plots (b)–(i) for ^{166}Er . The PT-plots focus on the part of the PES limited by the rectangle visible in panel (a). As an example of PT-plot, panel (c) depicts the 0_3^+ state against the 0_1^+ ground state chosen as a reference state (see the text).

if future experiments confirm the appearance of such a 0^+ state.

Figure 5(d) shows the PT-plot for the 0_3^+ state, indicating that the superposition of various basis vectors occurs in a much more mixed way. Figure 5(e) presents another clear pattern that the 0_6^+ state carries a γ vibration on top of the 0_1^+ state. Figure 5(f) displays the PT-plot for the 2_1^+ states, which is almost identical to panel (b). Figure 5(g) indicates that the triaxiality of the 2_2^+ state is slightly enlarged compared to the 2_1^+ state [12]. As seen from Fig. 5(h), the 2_3^+ state presents the same β -vibrational structure as the 0_2^+ state, i.e. it belongs to the rotational band built on top of the latter. Figure 5(i) depicts that the 4_7^+ state is the $J^P = K^P = 4^+$ rotation of the almost same triaxial intrinsic state as the ground and gamma bands. A recent experiment indicates that the $B(E2; 4_{\gamma\gamma}^+ \rightarrow 2_2^+) \sim 8.4$ W.u. is in a good agreement with the present calculation (see Fig. 4(b)) [56].

In summary, a novel picture of vibrational modes in strongly deformed heavy nuclei, at excitation energies below few MeV, was presented. Besides triaxial states forming the ground, γ , and $\gamma\gamma$ bands, a variety of vibrational bands generally appear. Their excitation energies are higher in most cases, except for the β band of ^{162}Dy . In the same energy region of such vibrational excitations, shape coexistence bands with similar β_2 values also appear, many of which may be of low excitation energies largely due to the self-organization [13]. The 0^+ state belonging to the γ -vibrational band decays rather strongly to the 2_{γ}^+ state. This

can be confused as the decay of a double γ phonon 0^+ state, but it is a single vibrational phonon excitation. Due to triaxiality, $K^P = 0^+$ vibrational band appears at lower energy than the corresponding $K^P = 2^+$ vibrational band. Eventually, a number of intriguing phenomena, including the appearance of low-lying states with stronger deformation than the ground state, provide potential fruitful agendas for carrying new nuclear spectroscopy experiments.

The authors are grateful to Dr. P. Van Duppen for valuable suggestions at early stage of the work, to Dr. A. Gorgen and Dr. M. A. Caprio for useful comments on vibrational modes, and to Dr. H. Ueno for continuous support to this research activity. TO thanks the visitor program of GANIL and the Alexander von Humboldt Foundation for the Research Award, as some parts of this work were made under their supports. TO is grateful to Dr. T. Kobori for encouraging remarks. The QVSM calculations were performed on the supercomputer Fugaku at RIKEN AICS (hp190160, hp200130, hp210165, hp220174, hp230207, hp240213, hp250224). This work was supported in part by MEXT as “Program for Promoting Researches on the Supercomputer Fugaku” (Simulation for basic science: from fundamental laws of particles to creation of nuclei, JPMXP1020200105, Simulation for basic science: approaching the new quantum era, JPMXP1020230411), and by JICFuS. This work was supported by JSPS KAKENHI Grant Number JP25K00998.

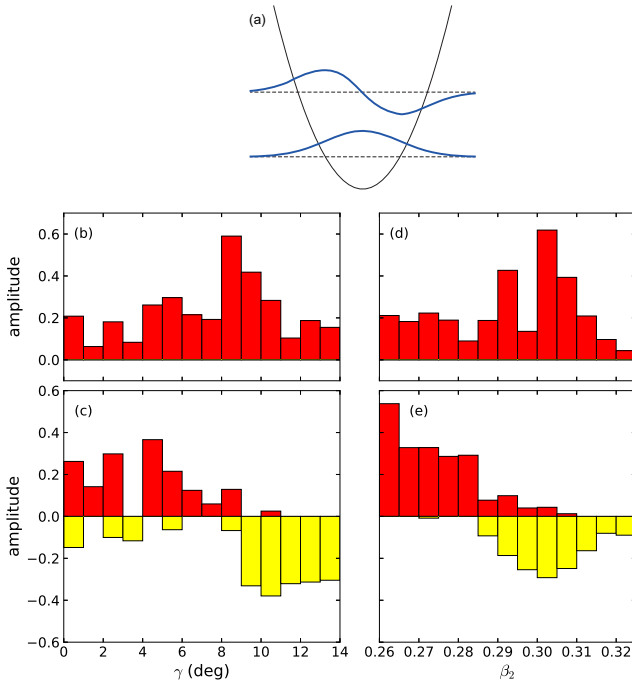


FIG. 3. (a) Schematic representation of the wave functions (blue solid line) and energies (black dashed lines) of the first two eigenstates of a particle in a one-dimensional harmonic oscillator potential. (b)–(e) Amplitude distribution per γ or β_2 bin. Red (yellow) histograms represent positive (negative) amplitudes for (b) 0_1^+ and (c) 0_3^+ states in ^{166}Er and for (d) 0_1^+ and (e) 0_2^+ states in ^{162}Dy .

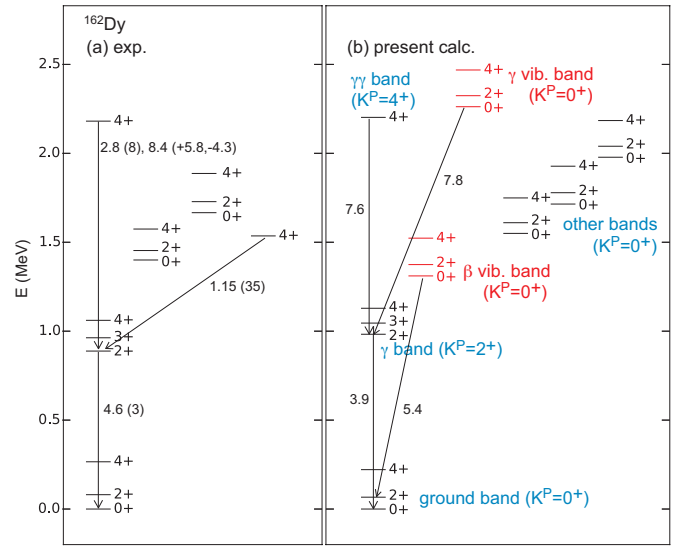


FIG. 4. Same as Fig. 1 for ^{162}Dy .

- * ytsunoda@nucl.ph.tsukuba.ac.jp
† otsuka@phys.s.u-tokyo.ac.jp
- [1] J. Rainwater, Phys. Rev. **79**, 432 (1950).
 - [2] A. Bohr, Mat. Fys. Medd. Dan. Vid. Selsk. **26**, 14 (1952).
 - [3] A. N. Bohr, *Nobel Lectures, Physics 1971–1980*, Editor Stig Lundqvist (World Scientific, Singapore, 1992); <https://www.nobelprize.org/prizes/physics/1975/bohr/facts/>.
 - [4] A. Bohr and B. R. Mottelson, Mat. Fys. Medd. Dan. Vid. Selsk. **27**, 16 (1953).
 - [5] A. Bohr and B. R. Mottelson, *Nuclear Structure* (Benjamin, New York, 1975), Vol. II.
 - [6] D. J. Rowe, *Nuclear collective motion: models and theory* (Methuen, London, 1970).
 - [7] A. De Shalit and H. Feshbach, *Nuclear Structure (theoretical Nuclear Physics)* (John Wiley and Sons, New York, 1974).
 - [8] M. A. Preston and R. K. Bhaduri, *Structure of the Nucleus* (Addison-Wesley, New York, 1975), Chap. 9.
 - [9] P. Ring and P. Schuck, *The Nuclear Many-Body Problem* (Springer-Verlag: Berlin, 1980).
 - [10] J. M. Eisenberg and W. Greiner, *Nuclear Theory*, 3rd ed., (North-Holland, Amsterdam, 1987), Vol. I.
 - [11] R. F. Casten, *Nuclear structure from a simple perspective* (Oxford University Press, New York, 2000).

- [12] T. Otsuka, Y. Tsunoda, N. Shimizu, Y. Utsuno, T. Abe, and H. Ueno, Eur. Phys. J. A **61**, 126 (2025).
- [13] T. Otsuka, Y. Tsunoda, T. Abe, N. Shimizu, and P. Van Duppen, Phys. Rev. Lett. **123**, 222502 (2019).
- [14] N. Shimizu, Y. Tsunoda, Y. Utsuno, and T. Otsuka, Phys. Rev. C **103**, 014312 (2021).
- [15] T. Otsuka, M. Honma, T. Mizusaki, N. Shimizu, and Y. Utsuno, Prog. Part. Nucl. Phys. **47**, 319 (2001).
- [16] N. Shimizu *et al.*, Prog. Theor. Exp. Phys. **2012**, 01A205 (2012).
- [17] S. Frauendorf, Int. J. Mod. Phys. E **24**, 1541001 (2015).
- [18] J. L. Wood, K. Heyde, W. Nazarewicz, M. Huyse, and P. Van Duppen, Phys. Rep. **215**, 101 (1992).
- [19] A. N. Andreyev *et al.*, Nature **405**, 430 (2000).
- [20] K. Heyde and J. L. Wood, Rev. Mod. Phys. **83**, 1467 (2011).
- [21] S. Leoni, B. Fornal, A. Bracco, Y. Tsunoda, and T. Otsuka, Prog. Part. Nucl. Phys. **139**, 104119 (2024).
- [22] B. A. Brown, Phys. Rev. Lett. **85**, 5300 (2000).
- [23] T. Otsuka, T. Suzuki, M. Honma, Y. Utsuno, N. Tsunoda, K. Tsukiyama, and M. Hjorth-Jensen, Phys. Rev. Lett. **104**, 012501 (2010).
- [24] T. Togashi, Y. Tsunoda, T. Otsuka, and N. Shimizu, Phys. Rev. Lett. **117**, 172502 (2016).
- [25] C. Kremer *et al.*, Phys. Rev. Lett. **117**, 172503 (2016).
- [26] T. Togashi, Y. Tsunoda, T. Otsuka, N. Shimizu, and M. Honma, Phys. Rev. Lett. **121**, 062501 (2018).
- [27] B. A. Marsh *et al.*, Nature Physics **14**, 1163–1167 (2018).
- [28] S. Sels *et al.*, Phys. Rev. C **99**, 044306 (2019).
- [29] Y. Tsunoda, N. Shimizu, and T. Otsuka, Phys. Rev. C **108**, L021302 (2023).
- [30] National Nuclear Data Center. Evaluated Nuclear Structure Data File. <http://www.nndc.bnl.gov/ensdf/>.
- [31] A. S. Davydov and G. F. Filippov, Nucl. Phys. **8**, 237 (1958).
- [32] A. S. Davydov and V. S. Rostovsky, Nucl. Phys. **12**, 58 (1959).
- [33] D. Cline, Ann. Rev. Nucl. Part. Sci. **36**, 683 (1986).
- [34] C. Fahlander *et al.*, Nucl. Phys. A **537**, 183 (1992).

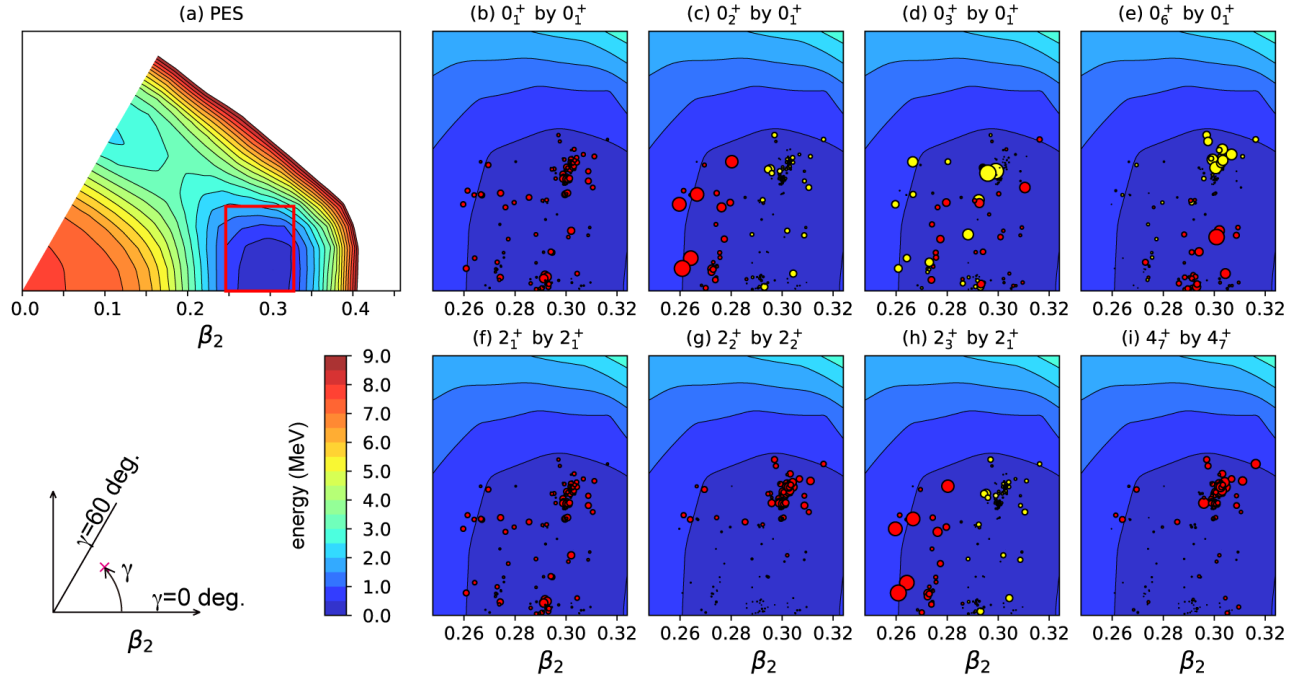


FIG. 5. Same as Fig. 2 for selected states in ^{162}Dy .

- [35] B. Kotliński *et al.*, Nucl. Phys. A **517**, 365 (1990).
 [36] Y. Sun, K. Hara, J. A. Sheikh, J. G. Hirsch, V. Velázquez, and M. Guidry, Phys. Rev. C **61**, 064323 (2000).
 [37] P. Boutachkov, A. Aprahamian, Y. Sun, J. A. Sheikh, and S. Frauendorf, Eur. Phys. J. A **15**, 455 (2002).
 [38] J.-P. Delaroche, M. Girod, J. Libert, H. Goutte, S. Hilaire, S. Péru, N. Pillet, and G. F. Bertsch, Phys. Rev. C **81**, 014303 (2010).
 [39] Z. P. Li, T. Nikšić, D. Vretenar, P. Ring, and J. Meng, Phys. Rev. C **81**, 064321 (2010).
 [40] J. F. Sharpey-Schafer, R. A. Bark, S. P. Bvumbi, T. R. S. Dinoko, and S. N. T. Majola, Eur. Phys. J. A **55**, 15 (2019).
 [41] Y. L. Yang, Y. K. Wang, P. W. Zhao, and Z. P. Li, Phys. Rev. C **104**, 054312 (2021).
 [42] S. P. Rouoof, N. Nazir, S. Jehangir, G. H. Bhat, J. A. Sheikh, N. Rather, and S. Frauendorf, Eur. Phys. J. A **60**, 40 (2024).
 [43] S. P. Rouoof, N. Nazir, S. Jehangir, G. H. Bhat, J. A. Sheikh, N. Rather, and S. Frauendorf, Phys. Rev. C **111**, 054309 (2025).
 [44] C. Fahlander, A. Axelsson, M. Heinebrodt, T. Hartlein, and D. Schwalm, Phys. Lett. B **388**, 475 (1996).
 [45] P. E. Garrett, M. Kadi, Min Li, C. A. McGrath, V. Sorokin, Minfang Yeh, and S. W. Yates, Phys. Rev. Lett. **78**, 4545 (1997).
 [46] P. E. Garrett, S. W. Wood, and S. W. Yates, Phys. Scr. **83**, 063001 (2018).
 [47] P. Möller, R. Nix, W. D. Myers, and W. J. Swiatecki, At. Data Nucl. Data Tables **59**, 185 (1995).
 [48] P. Möller, R. Bengtsson, B. G. Carlsson, P. Olivius, and T. Ichikawa, Phys. Rev. Lett. **97**, 162502 (2006).
 [49] Y. Tsunoda, T. Otsuka, N. Shimizu, M. Honma, and Y. Utsuno, Phys. Rev. C **89**, 031301(R) (2014).
 [50] T. Otsuka and Y. Tsunoda, J. Phys. G **43**, 024009 (2016).
 [51] Y. Utsuno, N. Shimizu, T. Otsuka, T. Yoshida, and Y. Tsunoda, Phys. Rev. Lett., **114**, 032501 (2015).
 [52] T. Otsuka, N. Shimizu, and Y. Tsunoda, Phys. Rev. C **105**, 014319 (2022).
 [53] D. J. Rowe, T. A. Welsh, and M. A. Caprio, Phys. Rev. C **79**, 054304 (2009).
 [54] D. J. Rowe and J. L. Wood, *Fundamentals of Nuclear Models: Foundational Models* (World Scientific, Singapore, 2010).
 [55] Y. Tsunoda and T. Otsuka, Phys. Rev. C **103**, L021303 (2021).
 [56] A. Aprahamian, C. Casarella, S. R. Leshner, K. Lee, B. P. Crider, M. M. Meier, E. E. Peters, F. M. Prados-Estévez, and Z. Tully, Eur. Phys. J. A **60**, 83 (2024).
 [57] States carrying larger J values are not shown for clarity.
 [58] The T-plot actually uses the β_2 and γ values computed of the vectors $|\phi^{(i)}\rangle$ [51, 52] because the orthogonalization linking both sets of states only involves states with very close values of the deformation parameters such that no significant changes of their values occurs between $|\phi_{iK}\rangle$ and $|\tilde{\phi}_{iK}\rangle$.
 [59] Essentially all significant contributions (i.e. circles) are located within this rectangle for all the eigenstates of present interest.
 [60] This constitutes the quantum mechanical equivalent of a classical particle at rest in the bottom of the well and a particle oscillating in the well, respectively.
 [61] The distribution of weights being asymmetric around the node, the vibration is somewhat anharmonic. This is consistent with the behavior of the PES in the β_2 direction.